Proceedings of ASME Turbo Expo 2004
Power for Land, Sea, and Air
June 14-17, 2004, Vienna, Austria

GT2004-53204

NUMERICAL INVESTIGATION OF UNSTEADY BOUNDARY LAYER TRANSITION INDUCED BY PERIODICALLY PASSING WAKES WITH AN INTERMITTENCY TRANSPORT EQUATION

Rene Pecnik, Wolfgang Sanz and Paul Pieringer
Institute for Thermal Turbomachinery and Machine Dynamics
Graz University of Technology
Graz, Austria
rene@ttm.tu-graz.ac.at

ABSTRACT

A numerical study was performed to investigate unsteady flow transition under the effect of periodically passing wakes on a highly loaded low-pressure turbine cascade. The simulation was done by a time-accurate 2D Navier-Stokes solver, which was developed at the Institute for Thermal Turbomachinery and Machine Dynamics. The transition process was modeled by coupling a baseline two-equation k-ω turbulence model with an intermittency transport equation via the turbulence production term.

The experimental investigations on the highly loaded low-pressure turbine cascade, called T106D-EIZ were carried out at the Institut für Strahlantriebe der Universität der Bundeswehr München (Germany). The available experimental data contains three test cases by varying the isentropic exit Reynolds number from 200.000 to 60.000.

The objective of this paper is to show the ability of an intermittency transport equation to model unsteady wake induced transition and separation mechanisms. The numerical results are compared by the pressure distribution, shape factor and loss behavior to the experiments.

INTRODUCTION

In turbomachinery and especially in aircraft engines the Reynolds numbers that determine the evolution of the boundary layers are relatively low. So a large part of the flow along the blade surfaces is laminar or transitional. The boundary layer development, losses, efficiency, heat transfer and boundary layer separation are greatly affected by laminar-to-turbulent transition. A great overview of the transition phenomena in turbomachinery was presented in the work of Mayle [1]. He recognized that three different modes of transition to turbulence may occur in boundary layer flows, natural, bypass and free shear layer transition above a laminar separation bubble. Due to the highly unsteady features in turbomachinery, Mayle speaks about "multi-mode" transition, induced by periodically passing wakes. This kind of unsteady transition is one of the main challenges for researchers.

The efficiency of the gas turbine critically depends on the low-pressure turbine (LPT). Hodson [2] reported that an increase in the efficiency of the LPT by 1% would improve the engine's fuel consumption by 0.5%. A further target is to reduce the blade count of a LPT, which also implicates reduced manufactured costs and decreased of engines weight. Cobley et al. [3] have shown that the blade count can be reduced by 20%, considering the unsteady transitional boundary layer, without significant efficiency losses. Therefore many experimental investigations were done on low-pressure turbine cascades with passing bar wakes to get an understanding of the flow physics. Experimental work was done by Stieger [4], who investigated the transition phenomena between wake passing events on a flat plate with a pressure gradient similar to the T106 LP cascade and on the LPT cascade itself. This work gives a detailed experimental insight into the unsteady transition mechanisms. Also DNS [5] on a flat plate with passing wakes and LES [6] on the T106 LPT cascade computations have supported a detailed insight into this flow.

The aim is now to incorporate these findings into Reynolds Averaged Navier-Stokes (RANS) solvers to improve the transition to turbulence predictions for engineering applications. The ability to accurately predict the transition process is crucial for the design of efficient and reliable machines. Considerable effort has been spent in improving the ability of different turbulence models to predict transition for various flows, by adding equations to e.g. standard k-ε turbulence models [7]. Beside these "pure" turbulence models, an increasing number of transition models are being developed from empirical correlations [8]. They are used to modify the turbulence models to better

predict the transition process. Most transition models are derived from boundary layer measurements on a flat plate and transition is described by an intermittency factor γ, which gives the fraction of time when the flow is turbulent. Whereas some numerical solvers incorporate algebraic intermittency models, recent approaches simulate transition to turbulence with intermittency transport equations [8][9]. These approaches allow to model transition for more general flows.

The objective of this work is to show the ability of an intermittency transport equation, originally developed by Steelant and Dick [8], for predicting unsteady transition on a highly loaded LPT cascade. Before investigating unsteady wake induced transition, two steady flat plate test cases were calculated. The turbulent quantities were calculated by the Menter SST [10] turbulence model. Laminar to turbulent transition was modeled by coupling the intermittency model with the production term of the Menter SST turbulence model. Two different approaches were investigated to overcome the excessive over prediction of turbulent kinetic energy at the stagnation point. The behaviors of these different approaches in conjunction with the intermittency model were evaluated by means of the skin friction distribution c_f over the first investigated flat plate case with zero pressure gradient. For the second flat plate test case with a non-uniform pressure gradient the authors postulate, that by matching the distribution of the free stream turbulence and the pressure gradient compared to the experiments, the transition model is able to predict the transition process correctly without a transition onset criterion.

For the unsteady simulations the LPT cascade T106D was chosen, where the numerical data are compared with the measurements provided by Stadtmüller [11] at the Institut für Strahlantriebe der Universität der Bundeswehr München (Germany).

NOMENCLATURE

A^+	=	Van Driest constant, A^+=26
c	=	chord length
c_f	=	skin friction, $c_f = \tau_w / \left(0.5 \rho_\infty U_\infty^2\right)$
H_{12}	=	shape factor
IM	=	intermittency model
k	=	turbulent kinetic energy [m^2/s^2]
M	=	Mach number
$\hat{n}\sigma$	=	turbulent spot growth parameter
P_k	=	turbulence production term [$kg/m/s^3$]
PRC	=	pressure correction parameter
Re	=	Reynolds number
S	=	magnitude of the strain rate [s^{-1}]
SST	=	Menter SST turbulence model
T	=	time scale bound
Tu	=	turbulence intensity, $Tu = 100 \cdot \sqrt{2/3\,k}\,/U$ [%]
U	=	amplitude of the velocity, $U = \sqrt{u^2 + v^2}$ [m/s]
y^+	=	dimensionless wall distance

Greek Letters

γ	=	intermittency factor
δ	=	boundary layer thickness [m]
λ	=	acceleration parameter
θ	=	momentum thickness
Ω	=	magnitude of the vorticity [s^{-1}]
ω	=	specific turbulent dissipation

Subscripts

1	=	inlet
2	=	outlet value
is	=	isentropic
le	=	leading edge
st	=	start of transition
w	=	value taken at the wall
ZPG	=	zero pressure gradient
∞	=	freestream, edge of the boundary layer

NUMERICAL METHOD

The flow solver used in this investigation was developed by Gehrer [12] and is a full Navier-Stokes code. The time iteration of the mean-flow and turbulence equations is done by an implicit scheme based on a Newton procedure and applying local time stepping. The Euler fluxes are discretized using a third-order TVD-upwind, cell-centered scheme based on Roe's approximate Riemann solver. The viscous fluxes are evaluated by central differencing.

TURBULENCE MODELING

The turbulent viscosity is modeled by the Menter shear stress transport (SST) k-ω turbulence model [10]. To avoid the excessive generation of turbulent kinetic energy in regions with large rates of strain (stagnation point), the turbulent time scale bound of Medic and Durbin [13] was applied, instead of the Kato and Launder [14] modification of the turbulent production term $P_k=\mu_t S\Omega$. The magnitude of the strain rate is defined as $|S|^2=2\cdot S_{ij}\cdot S_{ij}$, with $S_{ij}=1/2(\partial u_j/x_i+\partial u_i/x_j)$ and the magnitude of the vorticity as $|\Omega|=2\cdot\Omega_{ij}\cdot\Omega_{ij}$ with $\Omega_{ij}=1/2(\partial u_j/x_i-\partial u_i/x_j)$. Medic and Durbin summarized that this anomaly can be solved by modifying the turbulent production term, as proposed by Kato and Launder, or the turbulent dissipation. For the latter method the standard formulation of the turbulent production term is used, which leads to better behavior in simulating transition to turbulence with an intermittency model (see section below).

The turbulent viscosity is calculated by:

$$\mu_t = C_\mu \rho k T \tag{1}$$

where the time scale bound is defined as:

$$T = \min\left[\frac{1}{C_\mu \omega}, \frac{0.6}{\sqrt{6} C_\mu |S|}\right] \tag{2}$$

The main feature of the Menter SST model is the consideration of the transport of the shear stress in adverse pressure gradient boundary layers using the original correlation for the eddy viscosity. By applying the time-scale bound of Medic and Durbin the transport of the shear stresses would not be considered correctly. This aspect was not investigated in this work. Further by implementing the time scale bound into the turbulence model the dissipation equation changes, whereas the equation for the turbulent kinetic energy remains unaltered:

$$\frac{\partial \rho k}{\partial t}+\frac{\partial \rho u_j k}{\partial x_j}-\frac{\partial}{\partial x_j}\left[\left(\mu_l+\sigma_k \mu_t\right)\frac{\partial k}{\partial x_j}\right]=P_k-0.09\rho\omega k$$

$$\frac{\partial \rho \omega}{\partial t}+\frac{\partial \rho u_j \omega}{\partial x_j}-\frac{\partial}{\partial x_j}\left[\left(\mu_l+\sigma_\omega \mu_t\right)\frac{\partial \omega}{\partial x_j}\right]= \frac{1}{T}\left(\frac{c}{C_\mu k}P_k-\frac{\beta}{C_\mu}\rho\omega\right)+\left(1-F_1\right)\frac{2\rho\sigma_{\omega 2}}{\omega}\frac{\partial k}{\partial x_j}\frac{\partial \omega}{\partial x_j} \quad (3)$$

TRANSITION MODELING

The transition is modeled by coupling the turbulent production term P_k of the k and ω equations with the intermittency factor γ. Based on the idea of Lodefier et al.[15] following function was used:

$$P_k^* = \left(a+\left(1-a\right)\gamma\right)P_k \quad (4)$$

where the boundary layer detector a is defined as:

$$a=\min\left(1; b\left(\frac{U^2}{\nu\,\Omega\,10^5}\right)^4\right); \quad b=20 \quad (5)$$

This detector switches rapidly from zero within the boundary layer to one in the free-stream. In contrast to the suggestions of [15] the boundary layer detector a (Eq. 5) was modified by replacing the magnitude of the strain rate S with the magnitude of the vorticity Ω. As close to the stagnation point of the LPT blade the strain rate shows higher values in a more extended region, the boundary layer detector predicts a much thicker boundary layer. The substitution of the strain rate by the vorticity avoids this over-prediction of the boundary layer thickness at the stagnation region.

The intermittency model given in Eq. (6) corresponds to the equation, which is explained in detail in [8,15], except for the term R_γ, which was added by the authors as a first attempt to model relaminarization.

The transport for the intermittency equation reads:

$$\frac{\partial \rho \gamma}{\partial t}+\frac{\partial \rho u_j \gamma}{\partial x_j}-\frac{\partial}{\partial x_j}\left[\left(\mu+\frac{\mu_\gamma}{\sigma_\gamma}\right)\frac{\partial \gamma}{\partial x_j}\right]=(1-a)\left(C_P P_\gamma - C_R R_\gamma\right) \quad (6)$$

The source term of the intermittency model is multiplied with *(1-a)* to apply the growth of the intermittency only within the boundary layer, where a equals zero. By means of numerical calculation on the flat plate test cases the constant C_P was optimized to $C_P=1.35$, instead the original value of $C_P=2.0$ [15]. The intermittency production term P_γ was developed by Steelant and Dick [8] and was left unaltered in this work. Steelant and Dick derived the term P_γ from the intermittency distribution of Dhawan and Narasimha [16]. To further incorporate the effects of varying free-stream turbulence intensities and varying pressure gradients during transition, two widely known concepts can be applied. Solomon et al. [17] used a correlation for the variation of the half spreading angle and the propagation rate of the turbulent spots from experimental obtained data of the leading and trailing edge velocities of these turbulent spots. These correlations prescribe the growth of the intermittency during transition and depend on the pressure gradient parameter λ_θ. The second approach to incorporate varying pressure gradients was proposed by Steelant and Dick [8] on basis of Mayle's data [1] and is used in this investigation. They suggest a modified spot production rate in the production term P_γ according to following equation (7). The turbulent spot growth parameter for zero pressure gradient flows as proposed by Mayle [1] with $\hat{n}\sigma_{ZPG}=1.25\times10^{-11}Tu_\infty^{7/4}$ is modified using the acceleration parameter K.

$$PRC=\frac{\hat{n}\sigma}{\hat{n}\sigma_{ZPG}}=\begin{cases}\left(474\,Tu_{le,\infty}^{-2.9}\right)^{1-\exp(2\times10^6 K)} & K<0\\ 10^{-3227\,K^{0.5985}} & K>0\end{cases} \quad (7)$$

$$K=-\frac{\mu_\infty}{\rho_\infty^2 U_\infty^3}\frac{\partial p}{\partial x_j}. \quad (8)$$

The quality of transition predictions depends on determining the start of transition and thus on the correct determination of the local free-stream turbulence intensity. Compared to Steelant and Dick [8], we have taken the free-stream turbulence intensity direct from the turbulence model at the edge of the boundary layer by $Tu_\infty=\sqrt{2/3\cdot k_\infty}/U_\infty$ in order to account the decay of turbulence in the free-stream. A further reason to taking the turbulence intensity direct from the turbulence model at the edge of the boundary layer is to take into account the passing wakes for unsteady wake induced transition.

A difficult task in modelling the transition process with intermittency equations arises in determining the edge of the boundary layer. As most of the transition onset criteria are based on integral parameters, such as the momentum thickness Reynolds number, it is necessary to determine the boundary layer thickness. This makes the implementation into 3D Navier-Stokes codes or into commercial flow solvers difficult. In this work we determine the edge of the boundary layer with following relations [18]:

$$G(y)=\frac{1}{\bar{y}}\int_0^{y_{\max}} y\,\Omega\left[1-\exp\left(-\frac{y^+}{A^+}\right)\right]dy \quad (9)$$

$$\delta=1.145\,y_{ls}; \quad where \quad G\rightarrow G_{\max}$$

If y denotes the distance normal to the wall, the value y_{ls} at which the function $G_{(y)}$ reaches its maximum is assumed as turbulent length scale. The boundary layer thickness is then obtained by $\delta=1.145\cdot y_{ls}$. All other flow quantities, which are needed by the transition model at the boundary layer edge (indicated by "∞"), were approximated by isentropic relations.

As was mentioned before, the term for relaminarization was added by the authors as a first attempt to model the decay of the intermittency in highly accelerated boundary layer regions. This term is not supported by experimental results yet, but it will be a chance for future improvements. Fernholz and Warnack [19] have experimentally investigated accelerated turbulent boundary layers around axisymmetric bodies in a wind tunnel. The data are available at the ERCOFTAC database. This work could by a basis for the empirical modeling of the intermittency decay in strongly accelerated regions. However, we propose following term for relaminarization:

$$R_\gamma = \begin{cases} \gamma K_{Relam} \dfrac{\rho_\infty^2 U_\infty^2}{\mu_\infty} & K \geq K_{Relam} \\ 0.0 & K < K_{Relam} \end{cases} \qquad (10)$$
$$K_{Relam} = 3 \cdot 10^6$$

where K_{Relam} corresponds to the relaminarization acceleration parameter, as proposed by Mayle [8]. The constant C_R was set to 25, determined by numerical optimizations. We observed that this term should also depend on the free-stream turbulence intensity, the acceleration parameter and the Reynolds number. The primary function of R_γ is to reduce the intermittency downstream of the stagnation point of a LPT blade, where the model predicts high production of γ due to the high turbulence intensity up to 20%. Downstream of the stagnation point of a turbine blade the acceleration parameter is much bigger than K_{Relam} and thus the relaminarization start.

FIRST STUDIES

Before simulating unsteady wake passing transition, preliminary studies were performed on adiabatic flat plate test cases with sharp leading edges obtained from the ERCOFTAC SIG10 [20] database. The transitional boundary layer was calculated for two test cases, the T3A case with zero pressure gradient and the T3C2 case with a non-uniform pressure gradient. The data of the cases are summarized in table 1, where U_i is the inlet velocity, Tu_{le} the free-stream turbulence intensity at the flat plate leading edge. To match the decay of turbulence with the experimental data the mixing length lm_{le}, given in the last column of table 1, was specified.

	U_i [m/s]	Tu_{le} [%]	lm_{le} [mm]
T3A	5.4	3.35	0.94
T3C2	5.3	2.8	0.77

Tab. 1: Calculated flat plate test cases

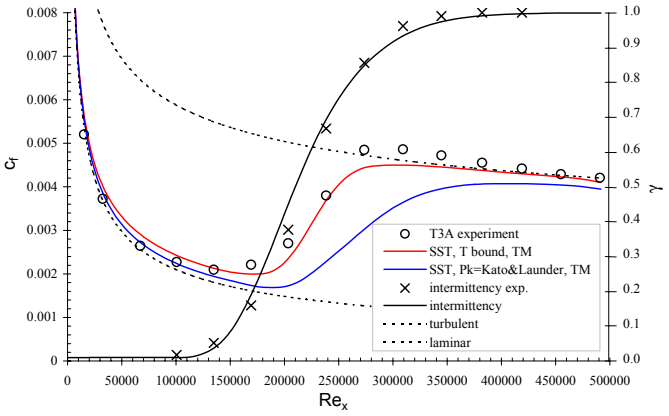

Fig. 1: Skin friction distribution and intermittency for T3A

Figure 1 shows the obtained results of the skin friction distribution for the T3A test case with the intermittency model coupled with the Menter SST k-ω model. The intermittency distribution (black solid line) agrees very well with the experimentally obtained distribution of γ. The Mayle [1] criterion was used to determine the start of transition, $\mathrm{Re}_{\theta,st} = 420 \cdot Tu_{le,\infty}^{-0.69}$. By coupling the Menter SST turbulence model via the production term with the calculated γ distribution, the different behaviors of the production terms can be seen very clearly. The red line shows the result with the applied time scale bound on the turbulence model and the standard production term, where the computed result matches the experimental values of the skin friction very well. By coupling the Kato and Launder turbulence production term with the same distribution of the intermittency, the skin friction shows a delay of the transition onset and a remarkably longer transition zone. Therefore the approach of Medic and Durbin was applied to the turbulence model, to overcome the stagnation point anomaly at the later investigated turbine cascade.

The second investigated case with a varying pressure gradient over the flat plate is shown in Fig. 2. In comparison to the T3A test case we modeled the test case T3C2 without a transition onset criterion. For the T3A test case with a zero pressure gradient distribution along the flat plate, an onset criterion is indispensable. But if the plate is subjected to a pressure gradient we observed that the intermittency model is able to capture the transition process correctly without a transition onset criterion. This is made possible by the pressure correction parameter *PRC*, which dampens the spot production rate in accelerated flow regions and thus causes that the intermittency growth slowly. In a decelerated flow region the spot production rate increases strongly, leading to a fast transition to turbulence as shown in Fig. 2. This approach worked also well for the cascade test cases with their rapidly changing pressure gradients. Further investigations will be performed to verify the applicability of this approach. Due to this good agreement for the T3C2 test case we also simulated the latter test case without a transition onset criterion.

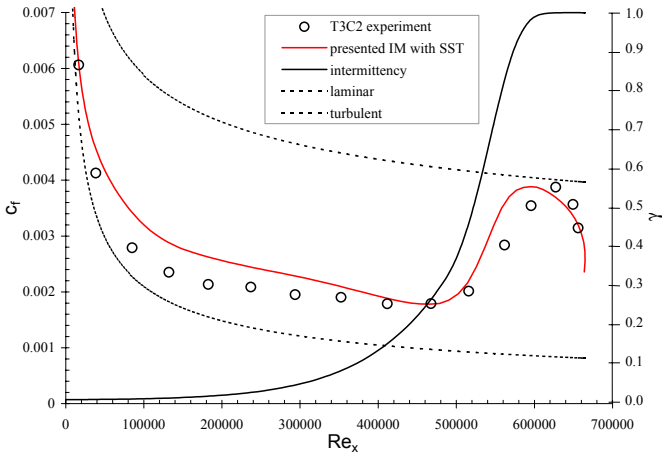

Fig. 2: Skin friction and intermittency distribution for T3C2

DESCRIPTION OF THE TEST CASE T106D-EIZ

The final numerical investigation of the ability to predict unsteady wake-induced transition with an intermittency transport model was done at the test case T106D-EIZ. This case was experimentally investigated in the high-speed cascade wind tunnel of the Universität der Bundeswehr München. The cascade profile represents the mid-span section of the PW2037

LPT rotor blade. At the experiment the pitch-to-chord ratio was increased from c/l=0.799 (original design) to c/l=1.05, in order to obtain a larger separation bubble on the suction side at approximately x/l_{ax}=0.6 for more detailed investigations. The main aim of the test rig is to study the influence of unsteady inflow conditions on the cascade blade row. The unsteady inflow is provided by moving bars, located 70mm upstream of the cascade inlet. The bar diameter corresponds to d_b/l_{ax} = 0.02 and the speed of the translation parallel to the cascade inlet plane equals 21.4 m/s.

The available test case documentation [11] contains three different operating points by varying the exit chord length Reynolds-number and the isentropic outlet Mach number. In this work the operating point 1 was simulated. The most important data are given in table 2.

	Re_{2c}	Ma_{2is}	U_b [m/s]	P_{t1} [bar]
Point 1	200000	0.4	21.4	0.2596

Tab. 2: Numerically investigated operating condition

Without the moving bars at this operating point the experiment indicates a large separation bubble, after $x/l_{ax} \approx 0.6$ as already mentioned before. By unsteady inlet conditions an up and downstream migration of the separation bubble was observed.

For the numerical investigations the geometric inflow angle β_1 was taken from Cardamone et al. [21] with β_1=41.6 for steady and unsteady simulations (see Fig. 3). Some difficulties arise by identifying the free-stream turbulence intensity Tu_1. By the simulations of Cardamone et al. the background turbulence level was set to Tu_1=0.8%, whereas in the test case documentation the turbulence level is given by Tu_1=2.5%. After communication with Hilgenfeld from the Universität der Bundeswehr München we define Tu_1 to 2.5%.

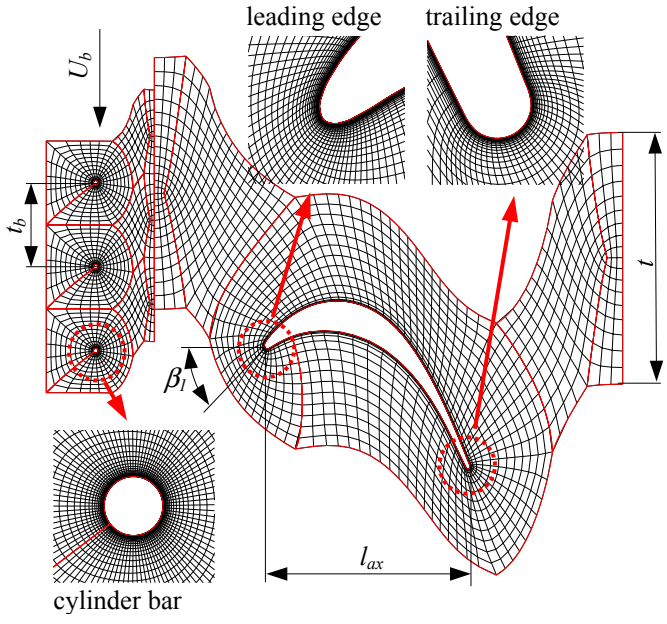

Fig. 3: Computational domain for T106D-EIZ

The computational grid is shown in Fig. 3. In each direction every fourth node is shown for the complete computational domain for visibility. The cylindrical bar, the leading and the trainling edge are shown largely magnified. Similar to Cardamone et al. the bar pitch t_b was reduced to 35mm (original 40mm) to obtain a multiple of the blade pitch of 105mm. The computational domain contains 12 blocks with a total of 49584 cells. The maximum value of y^+_{max} at the first cell-row at the walls is less than 0.4. The unsteady calculations were carried out using a second-order-accurate implicit time integration scheme. For passing of three bars 45000 time steps were applied.

RESULTS OF THE CASCADE TEST CASE T106D-EIZ

Figure 4 shows the distribution of the turbulent kinetic energy close to the leading edge and at the suction side from x/l_{ax}=0.62 till to 0.76 for the steady simulation without moving bars. The streamlines indicate four separation bubbles (marked with black arrows) in quick succession on the leading edge. The large separation results as the intermittency model predicts no transition onset. Because the first approach for the relaminarization term suppresses the growth of the intermittency in this region too much. Therefore in the free shear layer at the leading edge no increase of turbulent kinetic energy is noted. The black arrow in the right part of Fig. 4 indicates the separation bubble on the suction side, as was already observed at the experiments. This shows the ability of the transition model to predict a correct transition to turbulence, even in a separated shear layer, without a transition onset criterion.

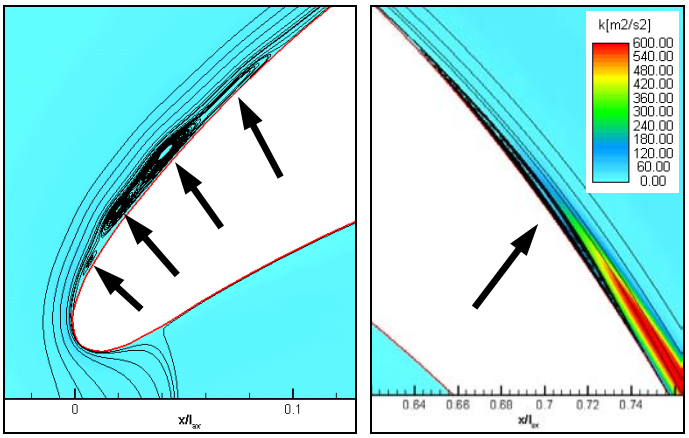

Fig. 4: steady distribution of the turbulent kinetic energy k [m²/s²]

Compared to the experiments by means of the isentropic Mach number distribution in Fig. 5 the steady numerical distribution deviates at the leading edge due to the afore mentioned large separation region. This prediction affects the pressure distribution downstream of the leading edge, whereas the isentropic Mach number distribution is predicted too low. The kink in Ma_{is} provoked by the separation bubble at x/l_{ax}≈0.7 matches the experimental values well. On the pressure side both simulations (steady and unsteady) capture the measured data in good agreement. On the suction side the unsteady time averaged distribution of Ma_{is} deviates remarkably from the measured one. The reason for this disagreement will be discussed later (Fig. 7).

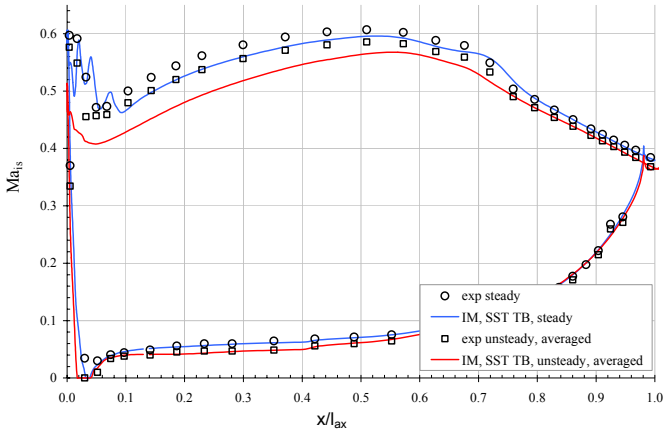

Fig. 5: Calculated isentropic Mach number distribution for steady and unsteady simulations

Figure 6 shows the wall shear stress at the blade profile along the suction side. As there are no measured data available a comparison between the computation and the experiment cannot be done. For the steady calculation the intermittency model predicts the onset of transition at approximately x/l_{ax}=0.62. Before the transition onset the laminar boundary is not able to withstand the adverse pressure gradient, which results in a detachment of the shear layer. This can be seen clearly by the negative values of the wall shear stress (red line). After this position the intermittency model predicts an increasing of γ, to a fully turbulent solution at x/l_{ax}=0.8 (dashed blue line). The resulting increase of the turbulent kinetic energy causes a turbulent reattachment of the detached shear layer, at approximately x/l_{ax}=0.76. If the blade is subjected to wake passing, the time averaged wall shear stress (blue line) shows nearly a complete suppression of the separation. As would be expected the corresponding time averaged intermittency distribution γ for the unsteady simulation shows a slightly more downstream transition, compared to the steady simulation. Also the leading edge separation bubbles (x/l_{ax}<0.1) vanish due to the periodically incoming wakes. Additionally the time averaged intermittency distribution shows a local peak of γ=0.1 at the leading edge, also caused by the wakes.

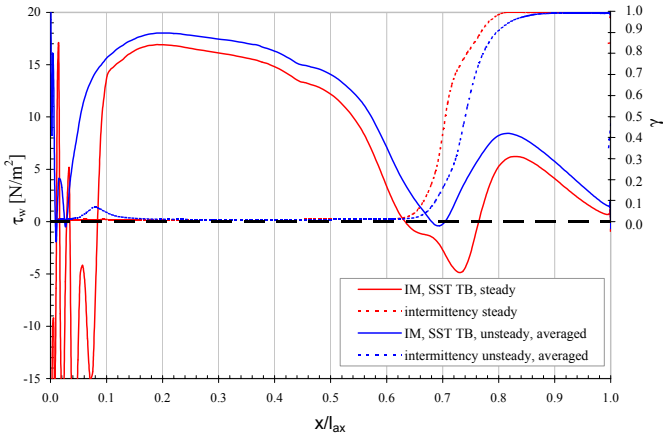

Fig. 6: Wall shear stress distribution for steady and unsteady simulations

Figure 7 shows the temporal development of the turbulent kinetic energy k for eight time instants during a bar passing period. The turbulent kinetic energy is drawn in the z-axis, giving a more vivid display of k, shown on the coordinate system on the last slide at the left upper corner. The arrows on the left of the first slide marked with "1" indicate two cylinder bars and their wakes, which convects downstream into the blade passage. The arrow marked with "2" shows the local peak of k, caused by the transition onset, on the suction side of the turbine blade. The time development of turbulent kinetic energy within the boundary layer on the suction side shows the decrease of the k maximum in magnitude and a migration downstream, as the influence of the wake vanishes. By the next wake passing event the turbulence of the wake diffuses into the boundary layer and this moves the transition onset upstream and increases the maximum of the turbulent kinetic energy again. This more upstream transition onset results in a complete suppression of the separation bubble, as will be shown later.

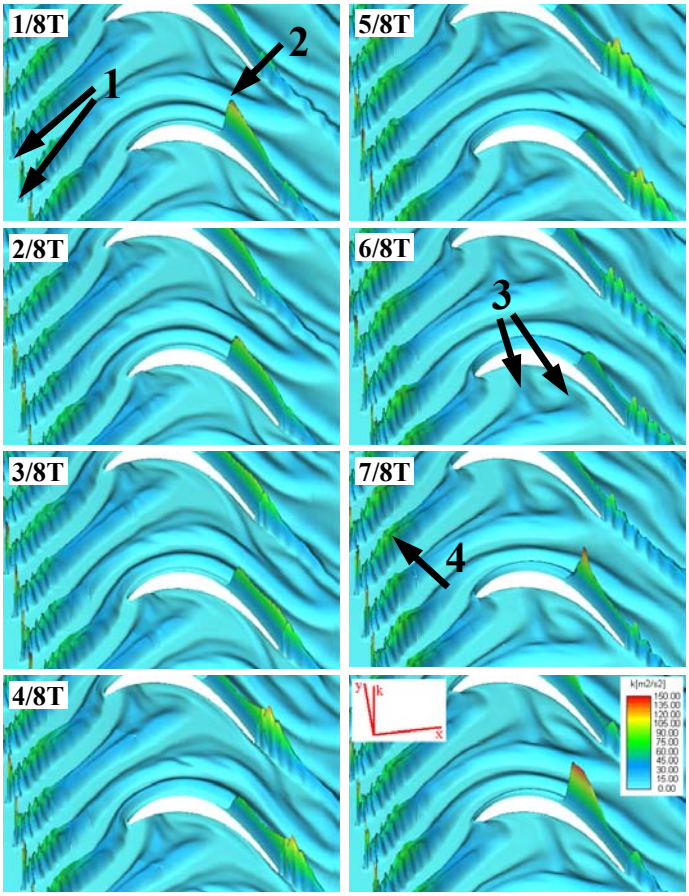

Fig. 7: temporal development of the turbulent kinetic energy

The computed wake development trough the blade passage agrees qualitatively to the experimental result of Stieger [4], who measured the turbulent wake convection through the T106 turbine cascade. The bowing, elongation and stretching of the wakes as predicted by the numerical solver agree well with the reported experimental data. The two arrows denoted with "3" indicate the local maxima of k, associated with the counter-rotating vortices.

The disagreement in the unsteady averaged isentropic Mach number distribution on the suction side, as mentioned

before (Fig. 5), may be explained by the too low turbulent kinetic energy behind the cylinders (arrow "4"). This results from the applied time scale bound of Medic and Durbin [13], which calculates significantly lower turbulent kinetic energy k compared to a calculation with the modified turbulent production term of Kato and Launder (not shown). It is interesting that with increasing distance behind the cylinder the turbulent kinetic energy k remains constant or even increases (arrow "4"). However the large extended region of the wake in stream direction yields in the wrong prediction of isentropic Mach number in Fig. 5. A further uncertainty, which can also cause an underprediction of the eddy viscosity, results from the estimation of the mixing length lm at the inlet. At the current simulation lm was determined to 1% of the blade pitch.

Figures 8 a, b and c, give a detailed insight into the computed time resolved distributions of the turbulence intensity Tu_∞ at the edge of the boundary layer, the intermittency γ and the time development of the skin friction coefficient c_f for the suction side of the blade. In order to facilitate interpretation the data for one wake passing period was copied onto the ordinate for three periods, whereas the abscissa corresponds to the non-dimensionalized axial chord length. As mentioned before the boundary layer edge turbulence intensity in Fig. 8a was directly obtained from the turbulence model by the relation, $Tu_\infty = 100 \cdot \sqrt{2/3\, k_\infty} / U_\infty$. The incoming wake hits the leading edge and is easily identifiable by the local maximum of the free-stream turbulence intensity (A). This is also apparent in Fig. 8c as the two small separation bubbles (B) disappear when the wake is present. The temporal distribution predicts, that the wake affects the boundary layer for more than half a wake passing period, as can be seen by the broad green region in Fig. 8a. Between the wakes in the mid of the suction side the turbulence intensity reaches its minimum of $Tu_\infty \approx 1.0$. The curved dashed line indicates approximately the maximum of the turbulence intensity (labeled with wake path). This wake path was transferred onto the figures on the right side. The time development of the intermittency γ shows a variation of the transition onset location between 0.56 and 0.62 chord length and is thus earlier than in the measurements of Stadtmüller et al. [22], although the range of the onset location variation is very similar. A very different result is published by Cardamone et al. [21] (not shown) who predict transition onset between 0.62 and 0.95 axial chord length. If the wake is present the transition onset occurs approx. at x/l_{ax}=0.6 and the reattachment location of the separation bubble (E) moves upstream until the separation bubble completely disappears. The black lines in Fig. 8c correspond to the qualitatively obtained time distribution of separation point (SP) and the reattachment point (RP) of the separation bubble from the experiments. The calculated position of the separation bubble agrees to the experiment, although the measurements do not show a disappearance of the separation bubble. Furthermore, the intermittency distribution shows an earlier laminar-to-turbulent transition in the time interval after the wake passing (labeled with "C"), which is approximately bounded by the wake path and the above dashed line (trailing edge of turbulent spots). Not well pronounced, but also visible in Fig. 8c is the region of the calmed boundary layer (labeled with "D"), where the intermittency shows a downstream movement of transition. This region is characterized by a laminar like but more stable velocity profile.

The serrated contours of the computed free-stream turbulence intensity of the skin friction are of the same frequency as the vortex shedding of the cylinder bars. The intermittency (Fig. 8b) distribution does not show this behavior so clearly, which indicates that the transition model reacts to slow for these instantaneous effects.

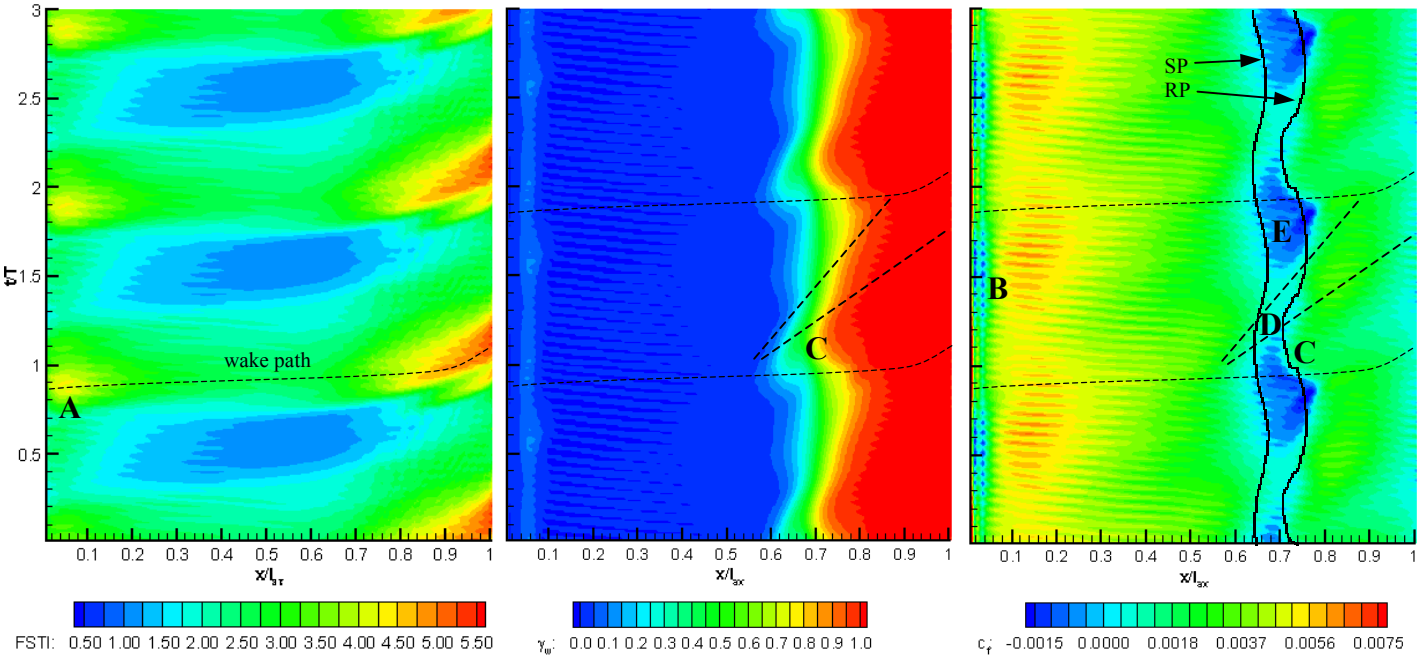

Fig. 8a: S-T diagram of FSTI

Fig. 8b: S-T diagram of the intermittency γ

Fig. 8c: S-T diagram of the skin friction c_f

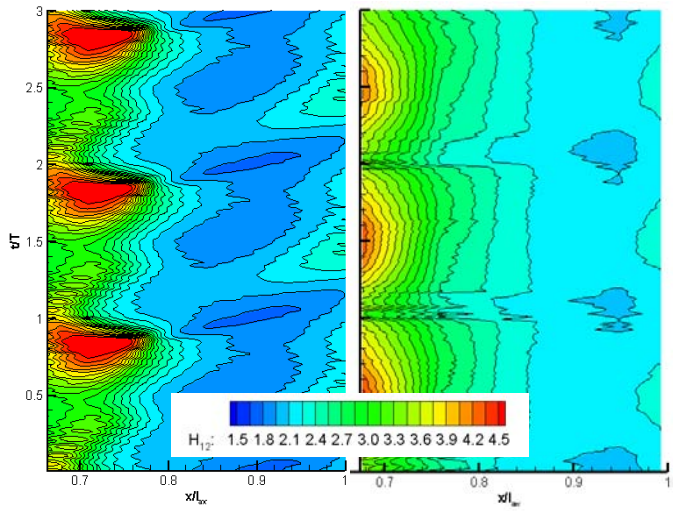

Fig. 9: Comparison of the shape factor H_{12} between the calculation (left) and the measurements (right)

Figure 9 shows a qualitative comparison between the calculated and the measured time development of the shape factor H_{12}. As the experimental data is only available for the rear part of the suction surface, the plot is restricted to this area. The shape factor is defined as the ratio of the displacement thickness and the momentum thickness of the boundary layer and gives the fullness of the boundary layer. Near the trailing edge (80% of the suction side) the computed values nearly correspond to the experimental values. The regions of low values of H_{12} are at the same position at x/l_{ax}=0.9, but deviate in magnitude. The computed high levels of H_{12}, which indicate the separated regions, are located more downstream and are less extended for one wake passing period compared to the experiments.

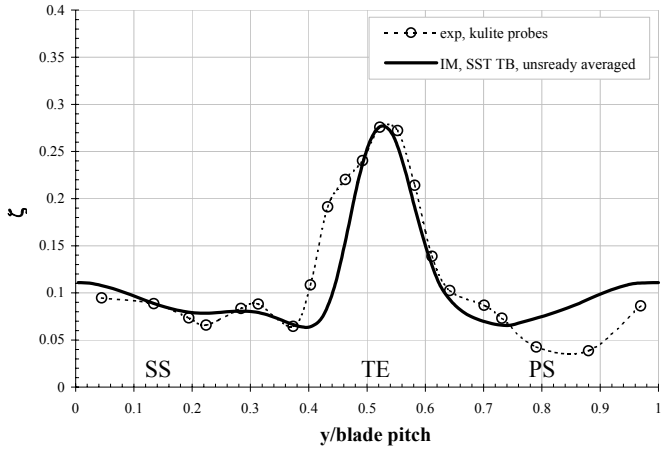

Fig. 10: Total pressure loss coefficient at 40mm downstream of the cascade exit plane

The time averaged total pressure loss coefficient (Fig. 10.), defined $\xi = (p_{t1} - \overline{p}_{t,exit})/(p_{t1} - p_{exit})$, was measured along a cross section 40mm downstream of the cascade exit plane. The measured distribution was obtained with fast response Kulite sensors mounted on a wake rake [11]. The presented calculation predicts a narrower wake compared to the experiments, whereas the magnitude of the loss coefficient agrees well with the measurements, despite the wrong prediction of the cylinder wake. At *y*/blade pitch between 0.75 and 1.0 the presented calculation over-predicts the pressure losses.

CONCLUSION

A numerical investigation was done to predict unsteady transition under the effect of wake passing on a low-pressure turbine cascade. For the calculation of the turbulent viscosity the Menter SST model [10] was chosen. To overcome the excessive production of turbulent kinetic energy in stagnation regions the time scale bound of Medic and Durbin [13] was applied to the turbulence model.

The transition was calculated by an intermittency transport equation and was coupled via the production term of the turbulence model. As first test cases the transitional boundary layer was calculated for two flat plates, with zero and varying pressure gradients. For the case with a non-uniform pressure gradient, transition to turbulence was modeled without a transition onset criterion.

Finally, the predictions of the unsteady transitional flow around a LPT cascade were compared with the measurements. The result showed that the time scale bound, although suppressing the unsteady turbulence production in the stagnation region, too strongly dampens the turbulence in the cylinder wake flow. This results in a significant under-prediction of the isentropic Mach number along the suction side of the succeeding blade compared to the experiments. The prediction of the shape factor agrees well with the results of other numerical investigations, but differs to the experiments.

Because no transition onset criterion was used, the transition model tends to produce intermittency already at the stagnation point. Therefore, it was necessary to add a relaminarization term to the transition model, which on the other hand suppresses the turbulence production at the leading-edge separation bubbles for the LPT test case. In future work the relaminarization term will be improved based on measurement, because it offers the possibility to avoid a transition onset criterion.

ACKNOWLEDGMENTS

This work was supported by the Austrian Science Foundation (FWF) under the grant P16761 as well as by an internal scholarship of Graz University of Technology to the first author.

REFERENCES

1 Mayle, R.E., (1991), *The Role of Laminar- Turbulent Transition in Gas Turbine Engines, Journal of Turbomachinery*, Vol. 113, pp. 509-537.

2 Hodson, H.P., (1998), *Bladerow Interactions In Low Pressure Turbines, in VKI Lecture Series No. 1998-02, Blade Row Interference Effects Axial Turbomachinery Stages*, Von Karman Institute, Feb 9-12

3 Cobley, K., Coleman, N., Siden, G. and Arndt, N., (1997), *Design of new three stage low pressure turbine for BMW Rolls-Royce BR715 engine*, ASME 97-GT-419

4 Stieger, R.D., (2002), The Effects of Wakes on Separating Boundary Layers in Low Pressure Turbines, Ph.D. Cambridge University Engineering Department

5 Wu, X., Jacobs, R.G., Hunt, J.R.C., Durbin, P.A., (1999), *Simulation of boundary layer transition induced by periodically passing wakes*, J. of Fluid Mech., Vol. 398, pp. 109-153
6 Michelassi, V., Wissink, J.G., Rodi, W., (2003), *DNS, LES and URANS of Periodic Unsteady Flow in a LP Turbine Cascade: A Comparison*, Procceding of 5th European Conference on Turbomachinery 2003, March 17-22, Czech Republic, Praha
7 Wang, C., Perot, B., (2002), *Prediction of turbulent transition in boundary layers using the turbulent potential model*, Journal of Turbulence, Vol. 3, 022
8 Steelant, J. and Dick, E., (2001), *Modeling of Laminar-Turbulent Transition for High Freestream Turbulence*, Journal of Fluids Engineering, Vol. 123
9 Huang, P.G., Suzen, Y.B., 2000, *An Intermittency Transport Equation for Modeling Flow Transition*, AIAA Paper 00-0287
10 Menter, F.R., (1994), *Two-Equation Eddy-Viscosity Turbulence Models for Engineering Applications*, AIAA Journal, Vol. 32, No. 8, August, pp. 1598-1605
11 Stadtmüller, P., Fottner, L., (2001), *A Test Case for the numerical Investigation of Wake Passing Effects on a Highly Loaded LP Turbine Cascade Blade*, ASME 2001-GT-311
12 Gehrer, A., (1998), *Entwicklung eines 3d-Navier-Stokes Code zur numerischen Berechnung der Turbomaschinenströmung*, PhD Thesis at Graz University of Technology
13 Medic, G. and Durbin, P.A., (2002) Toward improved prediction of heat transfer on turbine blades, J. of Turbomachinery, 124:187-192
14 Kato, M. & Launder, B.E., (1993), *Modelling Flow-Induced Oscillations in Turbulent Flow Around a Square Cylinder*, ASME FED, 157; 189-199
15 Lodefier, K., Merci, B., Langhe, D., C., Dick, E., (2003), *Transition modeling with the SST turbulence model and an intermittency transport equation*, Proceedings of ASME Turbo Expo. June 16-19, 2003, Atlanta, Georgia, USA, GT-38282
16 Dhawan, S., Narasimha, R., (1958), *Some Properties of Boundary Layer Flow During Transition from Laminar to Turbulent Motion*, Journal of Fluids Engineering, Vol. 3, pp. 418-436.
17 Solomon, W.J., Walker, G.J., Gostelow, J.P., (1996), *Transition Length Prediction for Flows With Rapidly Changing Pressure Gradients*, Transactions of the ASME, Vol. 118, pp 744-751.
18 Baldwin, B.S., Lomax, H., (1978), *Thin layer approximation and algebraic model for separated turbulent flows*, AIAA, paper 78-257.
19 Fernholz H.H. and Warnack D., (1998), *The effects of a fvourable pressure gradient and of the Reynolds number on an incompressible axisymmetric turbulent boundary layer*. Part 2. The boundary layer with relaminarization. J. Fluid Mech. 359, 357-381.
20 Savill, A M., (1992), *A synthesis of T3 Test Case Predictions, Numerical Simulation of Unsteady Flows and Transition to Turbulence*, O. P. et al., ed., Cambridge University Press, pp. 404-442.
21 Cardamone, P., Stadtmüller, Fottner, L., (2002), *Numerical Investigation of the Wake-Boundary Layer Interaction on a Highly Loaded LP Turbine Cascade Blade*, Procceding of ASME Turbo Expo 2002, June 3-6, Amsterdam, Netherlands, GT-30367
22 Stadtmüller, P., Fottner, L., Fiala, A., (2000), *Experimental and Numerical Investigation of Wake-Induced Transition on a Highly Loaded LP Turbine Cascade at Low Reynolds Numbers*, ASME Turbo Expo, May 8-11, Munch, Germany, GT-269